JOURNAL OF GEOPHYSICAL RESEARCH, VOL. 115, C01007, doi:10.1029/2008JC005264, 2010

Observation and modeling of platelet ice fabric in McMurdo Sound, Antarctica

D. E. Dempsey,[1] P. J. Langhorne,[1] N. J. Robinson,[2,3] M. J. M. Williams,[2] T. G. Haskell,[4] and R. D. Frew[5]

Received 31 December 2008; revised 20 July 2009; accepted 8 September 2009; published 26 January 2010.

[1] During the annual growth of landfast ice in McMurdo Sound, Antarctica, an episodic flux of platelet ice crystals from the ocean contributes to the build up of a porous subice platelet layer, which is steadily incorporated into the sea ice cover as it thickens over winter. In November 2007, we examined the spatial variability of these processes by collecting sea ice cores, with simultaneous oceanographic observations, along an east-west transect in the sound. Previously identified draped and bladed platelet ice types were observed. In addition, we identify resumed columnar growth which appears to be a result of geometric selection from the subice platelet layer after the arrival of new platelet crystals from the ocean has ceased. A numerical model of mechanical platelet ice processes is developed that predicts crystal texture and c axis distributions, producing virtual incorporated platelet ice with known growth history. This model demonstrates how a disordered subice platelet layer arises from an initially flat interface and suggests that such a layer is more likely to form later in the growth season. The model also suggests how the grain boundary density in incorporated platelet ice responds to changes in the flux of loose platelet crystals from the ocean. Application of this result to our 2007 platelet ice observations indicates that sea ice in western McMurdo Sound is subject to larger and more persistent platelet fluxes than the ice in the east. This is consistent with the pattern of in situ supercooling just beneath the ocean surface.

Citation: Dempsey, D. E., P. J. Langhorne, N. J. Robinson, M. J. M. Williams, T. G. Haskell, and R. D. Frew (2010), Observation and modeling of platelet ice fabric in McMurdo Sound, Antarctica, *J. Geophys. Res.*, *115*, C01007, doi:10.1029/2008JC005264.

1. Introduction

[2] There are two factors in the formation of Antarctic sea ice that cause its composition to differ from sea ice in the Arctic: the unconstrained and dynamic conditions of the Southern Ocean and the proximity of deep ice shelves [*Eicken and Lange*, 1989; *Hellmer*, 2004].

[3] The dynamic conditions of the marginal ice zone of the Southern Ocean result in a prevalence of granular ice types [e.g., *Eicken and Lange*, 1989; *Jeffries et al.*, 1997; *Worby et al.*, 1998]. Such a texture is displayed by grease ice, which is formed by the freezing together of frazil crystals that appear near the surface of the ocean as a result of rapid heat loss to the atmosphere [*Martin*, 1981; *Daly*, 2008]. In a wavefield, grease ice develops into an ice cover through the 'pancake cycle' [e.g., *Lange et al.*, 1989]. Accumulation of frazil beneath an ice cover indicates that conditions are stormy enough to transport frazil crystals from surface waters to depth [*Eicken and Lange*, 1989].

[4] Snow ice, formed when flooded snow refreezes, also displays a granular ice texture. Flooding usually occurs when the snow cover depresses the freeboard below sea level [*Jeffries et al.*, 2001]. Snow ice may be distinguished from the frazil or grease ice by its oxygen isotope signal ($\delta^{18}O$) [*Jeffries et al.*, 1994], where granular ice with $\delta^{18}O < 0$ is assumed to be snow ice, while that with $\delta^{18}O \geq 0$ is frazil ice [*Jeffries et al.*, 2001]. In contrast to the marginal ice zone, granular ice is less prevalent in the landfast sea ice of Antarctica. For example it contributes minimally (<3%) to the McMurdo Sound fast ice [*Jeffries et al.*, 1993; *Gow et al.*, 1998], probably because of the shelter provided by the Antarctic mainland and Ross Island.

[5] Ice shelves exist around 44% of the Antarctic coastline [*Drewry et al.*, 1982]. Ice shelf/ocean interactions result in the formation of platelet ice within the water column, which makes a significant contribution to the composition of coastal sea ice. In particular, theoretical studies estimate that ice shelf/ocean interaction may contribute up to 0.2 m of the sea ice thickness over significant areas of landfast and pack ice in the Southern Ocean [*Hellmer*, 2004]. Basal melting at the underside of ice shelves produces a body of relatively cool and fresh water that rises due to buoyancy. As pressure is released, the freezing point rises and the

[1]Department of Physics, University of Otago, Dunedin, New Zealand.
[2]National Institute of Water and Atmospheric Research Ltd., Wellington, New Zealand.
[3]Department of Marine Science, University of Otago, Dunedin, New Zealand.
[4]Industrial Research Ltd., Lower Hutt, New Zealand.
[5]Department of Chemistry, University of Otago, Dunedin, New Zealand.

0148-0227/10/2008JC005264$09.00

water becomes supercooled [*Foldvik and Kvinge*, 1974]. This mechanism is known as an ice pump [*Lewis and Perkin*, 1986] because ice crystals grow to relieve local supercooling, further increasing the local buoyancy, and forming an ice shelf plume [see, e.g., *Jenkins and Bombosch*, 1995; *Smedsrud and Jenkins*, 2004].

[6] In this paper we describe platelet ice in one of three environments under landfast sea ice. In the first, loose ice platelet crystals are suspended by turbulence or rise in the water column and are presumed to originate from interaction with an ice shelf. *Dieckmann et al.* [1986] and *Penrose et al.* [1994] observed loose platelets at depths as great as 250 m. In McMurdo Sound an episodic flux of these crystals has been inferred from observations of scatterers in the water column, which from mid-May 2003 appeared concurrently with surface supercooling [*Leonard et al.*, 2006].

[7] Second, the subice platelet layer is the name we shall use for a porous accumulation of platelets that have either grown at the ice-water interface [*Gow et al.*, 1998] or settled from the water column. Such layers have been observed in the Weddell Sea [*Eicken and Lange*, 1989], in the Ross Sea off Hells Gate Ice Shelf [*Tison et al.*, 1998], and in McMurdo Sound [*Littlepage*, 1965; *Crocker and Wadhams*, 1989; *Jeffries et al.*, 1993; *Gow et al.*, 1998; *Leonard et al.*, 2006], where thicknesses as large as 7 m have been observed below the multiyear ice (J. Leitch, personal communication, 2007). In these layers single platelet dimensions can be 100's of mm across and 2–3 mm thick. *Eicken and Lange* [1989] suggest that the presence of a subice platelet layer provides a buffer against basal melting of the sea ice in the summer. Such layers also exist under ice shelves where they are linked to marine ice: for example below the Amery Ice Shelf [*Craven et al.*, 2005, 2009].

[8] Third, the upper portion of the subice platelet layer is steadily incorporated into the overlying sea ice cover by the advancing ice-water interface and freezing in the platelet interstices [*Jeffries et al.*, 1993], forming incorporated platelet ice. A thin section of incorporated platelet ice reveals considerable variation in platelet size, shape and number density. This has led to the subclassifications; draped platelet ice, named for its resemblance to draped fabric and characterized by centimeter-sized crystals and curved grain boundaries [*Jeffries et al.*, 1993; *Tison et al.*, 1998]; and bladed platelet ice, characterized by vertically extensive, blade-like crystals and sharp grain boundaries, observed by *Eicken and Lange* [1989], *Gow et al.* [1998], *Tison et al.* [1998], and *Leonard et al.* [2006], although not termed as such. In McMurdo Sound *Gow et al.* [1998] concluded that incorporated platelet growth occurs entirely in situ and *Smith et al.* [2001] recorded video footage of platelets, attached at the interface, growing down into the ocean.

[9] This study examines the relationships between platelet ice in these three environments in the context of McMurdo Sound. We are interested in what can be inferred from the crystallographic structure of incorporated platelet ice, sampled at the end of its growth season, about the conditions in which it formed. This investigation begins with a summary of the macroscopic, textural and crystallographic ice characteristics from a coring survey of the McMurdo Sound annual fast ice, sampling six sites over a variety of platelet ice and oceanographic conditions. A new numerical model is then developed to explore the processes responsible for the variety of observed incorporated platelet ice fabrics. This model simulates the transfer of platelets from the water column to the subice platelet layer, and eventually into the structure of the sea ice. It predicts crystal texture and c axis orientations in virtual incorporated platelet ice. Comparison with corresponding observed quantities allows us to draw conclusions about the conditions present in the 2007 winter in McMurdo Sound.

2. Observations in McMurdo Sound

2.1. Platelet Abundance Distribution

[10] The presence of New Zealand and United States Antarctic bases in McMurdo Sound has resulted in it being the subject of a number of platelet ice observations, [e.g., *Hodgson*, 1907; *Wright and Priestley*, 1922; *Paige*, 1966; *Dayton et al.*, 1969; *Crocker and Wadhams*, 1989; *Jeffries et al.*, 1993; *Gow et al.*, 1998; *Smith et al.*, 2001; *Leonard et al.*, 2006]. We have built on this experience to determine the best locations for sampling.

[11] We have analyzed data from coring surveys carried out by *Gow et al.* [1998], *Jones and Hill* [2001], and *Jeffries et al.* [1993] (see Table 1) to determine a distribution of platelet abundance. The thickness of the incorporated platelet ice layer in a core, z_{ij}, is defined for the jth core location of the ith survey. To eliminate interannual and seasonal variability between surveys, the mean, $\overline{z}_i$, and standard deviation, σ_i, of the incorporated platelet ice thickness for each of the three surveys is used to calculate a normalized value, defined as $z'_{ij} = (z_{ij} - \overline{z}_i)/\sigma_i$, and termed relative platelet abundance. Values of z'_{ij} were sorted into one of five bins, of unit width, centered at [−2, −1, 0, 1, 2]. Contours of constant relative platelet abundance for McMurdo Sound are presented in Figure 1. A prominent tongue of high platelet concentration is seen along the western side of the Sound, which we presume to be the result of platelet crystals emerging from beneath McMurdo Ice Shelf and becoming incorporated in the sea ice cover. It corresponds to the contours of winter surface supercooling observed by *Lewis and Perkin* [1985], and with the subjectively assessed "platelet abundance index" of *Barry* [1988].

[12] The relative platelet abundance distribution of Figure 1 and an earlier version from *Langhorne et al.* [2006] served as the motivation for the location of survey sites of the 2007 field campaign.

2.2. Survey Location

[13] The first year sea ice, and the oceanography beneath it, were sampled along an east-west transect in McMurdo Sound. Six sites were visited between 16 November and 1 December 2007 at a spacing of approximately 5 km. The locations of these sites were chosen to sample sea ice over the range of relative platelet abundance shown in Figure 1. Classified by similarity in ice textures and salinity, the six cores are divided in two groups, the western cores comprising W1–W3 and the eastern cores comprising E1–E3 (see Table 2). From west to east, they are denoted W1, W2, W3, E1, E2 and E3.

2.3. Methods

[14] At each survey location three 80 mm diameter cores were extracted. Alignment with a true north azimuth was recorded for each core. Cores extracted for sea ice salinity

Table 1. Survey Statistics Used to Generate the Relative Platelet Abundance Map for McMurdo Sound

Source	Survey Date	Sites Surveyed	$\overline{z}_i$ (cm)	σ_i (cm)
Gow et al. [1998]	Oct–Nov 1980	25	26	10
Jones and Hill [2001]	Oct–Dec 1982	9	73	18
Jeffries et al. [1993]	Jan 1991	15	77	35

measurement were cut on site to 10 cm lengths, packaged in plastic pottles and transported to New Zealand's Scott Base for analysis. Salinity measurements were performed on a Wayne Kerr Automatic LCR meter using standard calibration solution and following procedures outlined by *United Nations Educational, Scientific and Cultural Organization* [1981].

[15] Two cores were taken for structural analysis. One core was cut vertically down its length to produce thick sections, ~10 mm thick, that indicate ice composition in transmitted light. At depths of interest horizontal and vertical thin sections, approximately 0.5 mm thick, were produced. These were photographed under crossed polarizers, which distinguished individual crystals by the orientation of their c axis (optic axis). For selected horizontal thin sections, the distribution of crystal c axis orientations was measured on a Rigsby universal stage and presented on a Schmidt equal area net following *Langway* [1958].

[16] Grain boundary density, B_A, defined by *Eicken et al.* [1994] as the length of grain boundary per unit area, was calculated for horizontal thin sections by manual digitization of grain boundaries in thin section images. This measure is sensitive to average grain size, shape and number density.

[17] Oceanographic measurements were collected at the same time as the ice cores, through a 250 mm diameter hole in the ice. At each site full depth conductivity-temperature-depth (CTD) profiles were taken to determine ocean temperature and salinity. In this paper we only report data collected close to the ice-water interface, the remainder will be presented elsewhere. At site E3 an oceanographic mooring was deployed between 16 November and 6 December, which measured temperature, salinity and current speed and direction at multiple depths. The record of the shallowest current meter at 63 m is of relevance to this study.

3. Observed Ice Characteristics

[18] The analysis of cores along the transect is complicated by breakout events that took place during winter, and it is very unlikely that freeze over took place at the same time at all sites. Consequently the age of the sea ice at each site is estimated using two methods: from satellite observations, and from a freezing degree day (FDD) calculation using the temperature record from the Arrival Heights weather station (see Figure 1). The dominant wind direction during sea ice growth was from the SSE (bearing 341°).

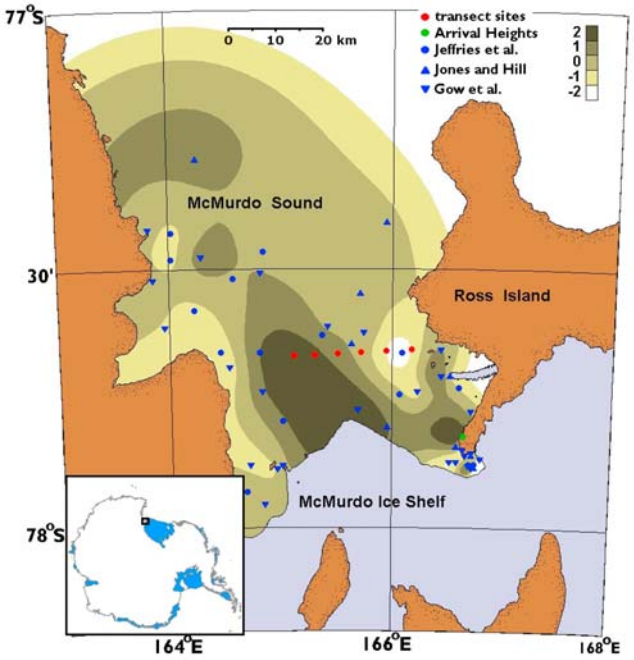

Figure 1. Map showing contours of relative platelet abundance in McMurdo Sound inferred from past surveys (shown by blue symbols). Red circles mark the location W1–E3 going left to right (west to east). The location of the Arrival Heights weather station is also shown.

3.1. Thickness: Snow, Ice, and Subice Platelet Layer

[19] At all sites surveyed the snow cover was light with a maximum of 7 cm at W2 and E1. Considerable amounts of sediment, up to 7 tonnes km^{-2} in southern McMurdo Sound (G. Dunbar, personal communication, 2007), were also observed mixed with snow. This indicates that the strong winds, responsible for carrying sedimentary material from land, are also responsible for the transport of snow and its limited build up.

[20] Ice thickness along the transect is shown in Figure 2. Ice thicknesses in the western Sound are consistent with relative freeze over dates according to DMSP satellite

Table 2. Summary of Sea Ice Sites Visited in 2007[a]

Site	Longitude (east)	Latitude (south)	Date Visited	Ice Depth (m)	$\overline{S}$	Satellite Freeze	FDD Freeze	S_w
W1	165° 06.678	77° 40.070	19 Nov	1.97	8.0	25–29 Jul	3–22 Jun	34.65
W2	165° 17.863	77° 39.977	20 Nov	1.65	7.7	11–25 Sep	13 Jun to 1 Aug	34.70
W3	165° 30.446	77° 39.846	22 Nov	1.05	8.3	11–25 Sep	17–28 Sep	34.69
E1	165° 42.983	77° 39.660	24 Nov	2.18	6.4	12–29 Apr	9 Mar to 21 May	34.70
E2	165° 56.784	77° 39.500	1 Dec	2.10	6.0	12–29 Apr	13 May to 6 Jun	34.69
E3	166° 10.585	77° 39.356	16 Nov	1.99	6.6	12–29 Apr	13 Apr to 19 Jun	34.65

[a]Mean ice salinity, $\overline{S}$, and salinity of upper 20 m of water column, S_w, shown along with approximate ice freeze over dates according to satellite images and a freezing degree day (FDD) calculation.

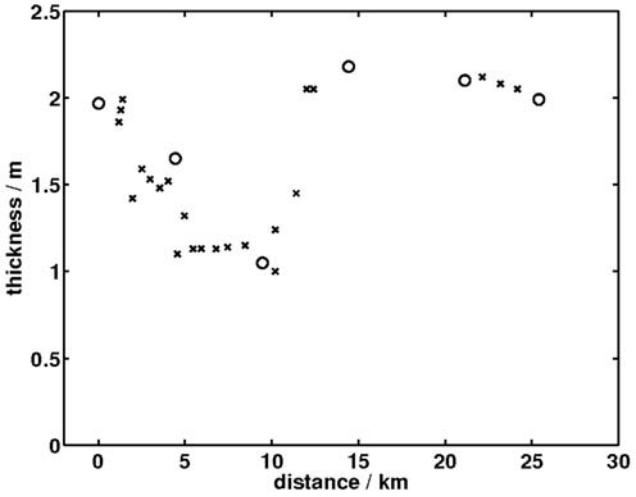

Figure 2. Ice thickness across transect. Sites W1–E3 are marked left to right by open circles with W1 marked at 0.

images (see Table 2). The freezing degree day calculation models the release of latent heat at the growing interface and its conduction through the sea ice to the atmosphere [*Maykut*, 1986]. In addition the transfer of latent and sensible heat between the upper ice or snow surface and the air is parameterized by an average heat transfer coefficient. As we have no record of snow depth with time during the growth season we have calculated limits for the freeze over dates based on the following two bounding assumptions: (1) that there was no snow cover and (2) that there was a cover of constant thickness at the value observed when we visited the site. Heat exchange with the ocean is assumed negligible. Freeze over dates from the two sources for W1 and W2 (see Table 2) differ by more than a month, indicating that there may have been a contribution to the thickness from sources not included in the FDD calculation, such as platelet incorporation or frazil herding by wave or tidal action [*Martin*, 1981].

[21] Conversely, freeze over dates from the satellite images and FDD calculations are in approximate agreement for the eastern cores. This suggests a reduced contribution to sea ice thickness from the ocean, in contrast with the western cores.

[22] The thickness of the subice platelet layer at each site is qualitatively inferred at the time of sampling. At some locations oceanographic access holes filled immediately with loose platelet crystals that had presumably been disturbed from a subice platelet layer directly beneath. Platelets were recovered from the hole, with a large volume removed at W1 and lesser amounts at W2 and W3. No platelets were observed emerging from holes drilled at E1, E2 or E3 indicating the absence of a subice platelet layer in these locations. This is consistent with the pattern of supercooling within the upper 20 m of the surface of the ocean at the time of sampling. On the western Sound, at W1 and W2, the upper ocean was supercooled by ~10's of mK (see Figure 4). At other sites, the water was above its freezing point, rising toward the eastern side of the Sound to a maximum of 0.2°C above freezing at E3 (see Figures 4 and 5).

3.2. Sea Ice Salinity

[23] Salinity-depth profiles for the six transect sites are presented in Figure 3. The younger ice at sites W2 and W3 exhibit prominent C-shaped profiles similar to those observed by *Nakawo and Sinha* [1981] in the Arctic for young first year sea ice. Sea ice salinities from E1–E3, which have been growing since mid-April, are similar in magnitude and depth dependence to those from ice of comparable age observed by *Gow et al.* [1998].

[24] Figure 3 shows there is a difference in mean salinity, defined as the salinity that would be obtained if the entire core was melted, between the western cores and the eastern cores. In particular, cores from W1 and E3 are of approximately the same length yet exhibit mean salinities of 8.0 and 6.6, respectively (see Table 2). There appears to be no correlation between upper ocean salinity (at the time cores were sampled) and mean core salinity (see Table 2). However, as detailed in section 3.1, W1 and E3 appear to

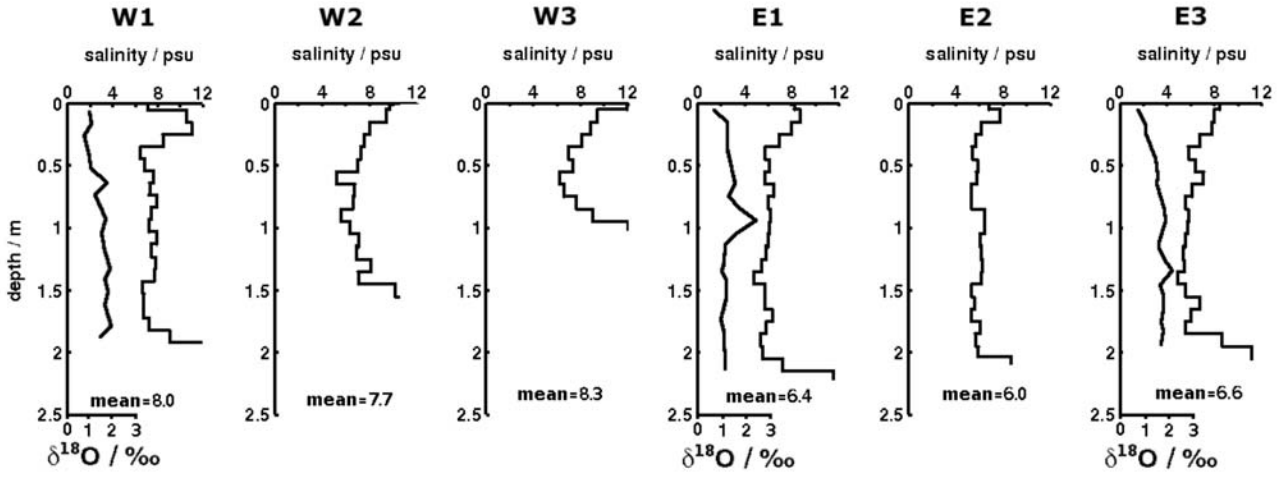

Figure 3. Sea ice salinity profiles from west to east across McMurdo Sound. Here $\delta^{18}O$ profiles are shown to the left of salinity profiles for W1, E1, and E3. Mean salinities are shown at the base of each profile.

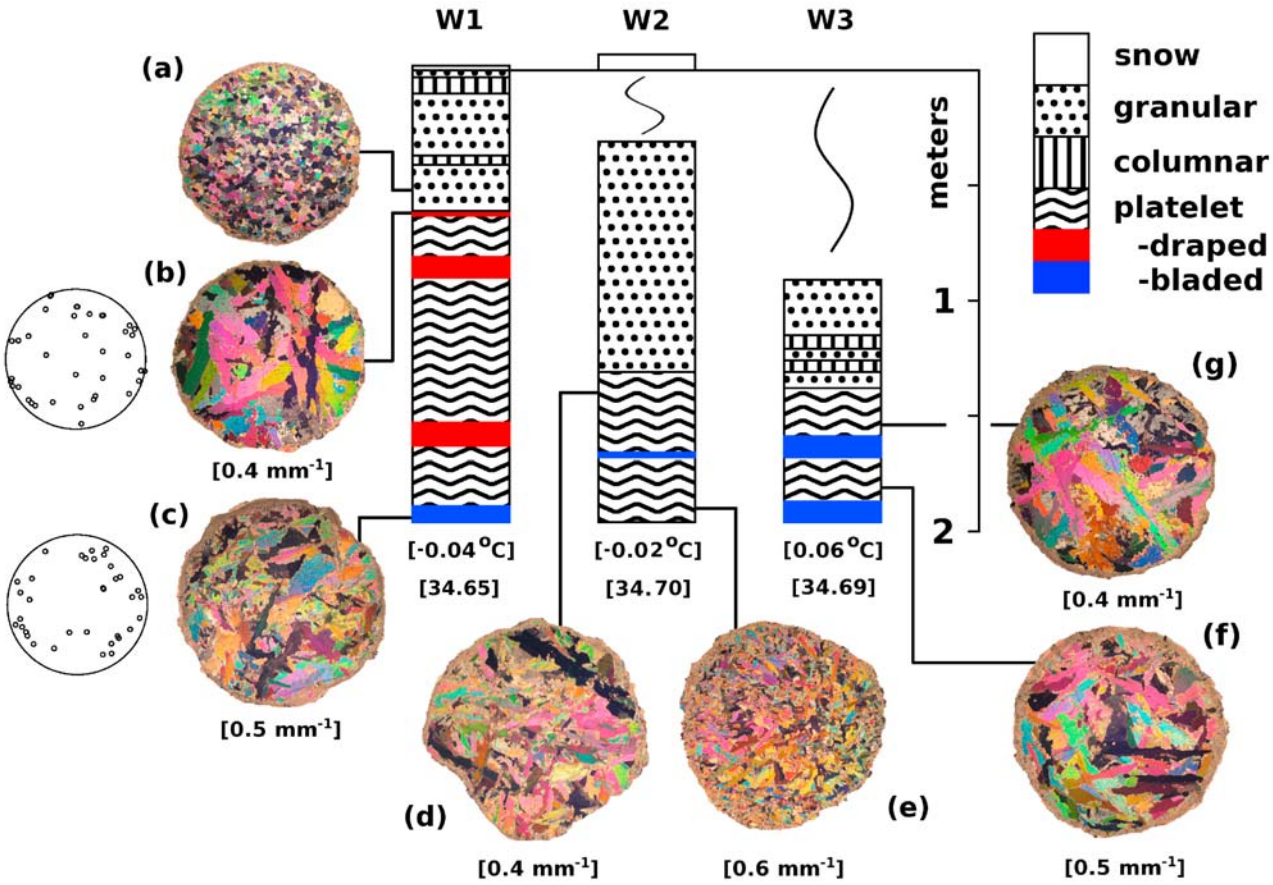

Figure 4. Ice composition summary and sample thin sections from western cores. (a) Granular texture, (b) draped platelet, (c and d) bladed platelet, (e) a mixture of granular texture and bladed platelet, and (f and g) bladed platelet. The deviation of the temperature from the in situ freezing point, averaged over the top 20 m of the water column, is presented below corresponding cores. Salinity averaged over the top 20 m of the water column is also shown. Where appropriate, B_A values for thin sections are included. Cores W2 and W3 are shorter than W1 because of later freeze over at these sites.

have considerably different growth histories. Sea ice at W1 froze later and grew more quickly than that at E3 due to the contribution of platelet incorporation and/or frazil herding. *Eicken* [1992], studying 14 predominantly columnar and 37 predominantly granular ice cores from the Weddell Sea has shown that there is no significant difference in mean core salinity between the ice types. We therefore attribute the apparently higher salinity of sea ice in western McMurdo Sound to the increased growth rates in this region.

3.3. Ice Composition

3.3.1. Granular Ice

[25] Profiles of $\delta^{18}O$ at W1, E1 and E3 (see Figure 3) indicate that, due to the absence of a negative signal at the top of the profile, snow ice is not a contributor to the sea ice at these locations. We attribute all small grained ice fabric to grease ice formation [*Martin*, 1981].

[26] Unusually large amounts of granular ice were observed in the western cores, contributing 31% to 61% of the total thickness (see Figure 4). On the other hand, Figure 5 shows only 0–10 cm (<5% of the total thickness) of granular ice preceding the columnar ice that dominates the next ~1 m in each of the eastern cores. This sequence is consistent with ice grown in relatively calm conditions [*Weeks and Ackley*, 1982].

3.3.2. Columnar Ice

[27] Granular ice that grows downward due to atmospheric heat flux develops into columnar ice, characterized by a lamellar texture. Ice plates are separated by rows of brine pockets, which arise because of an interface instability that occurs in conditions of constitutional supercooling [*Weeks and Ackley*, 1982]. The growing crystals are subject to geometric selection, which prefers those crystals with c axes close to the horizontal plane, and causes a girdle c axis distribution to develop (points distributed around the margin of a Schmidt net, see Figures 5g and 5h). Further alignment can occur within the horizontal plane due to a current at the interface, which confers a growth advantage to those crystals with c axes close to the current direction [*Weeks and Gow*, 1978; *Langhorne and Robinson*, 1986]. This causes a uniaxial girdle c axis distribution to develop.

[28] In 2007 columnar ice accounted for 44% of the eastern ice cores but only approximately 5% in the western cores (see Figures 4 and 5). Disagreement with past surveys, where columnar ice has been observed to contribute 60% to 72% of total ice thickness [*Jeffries et al.*, 1993; *Gow et al.*,

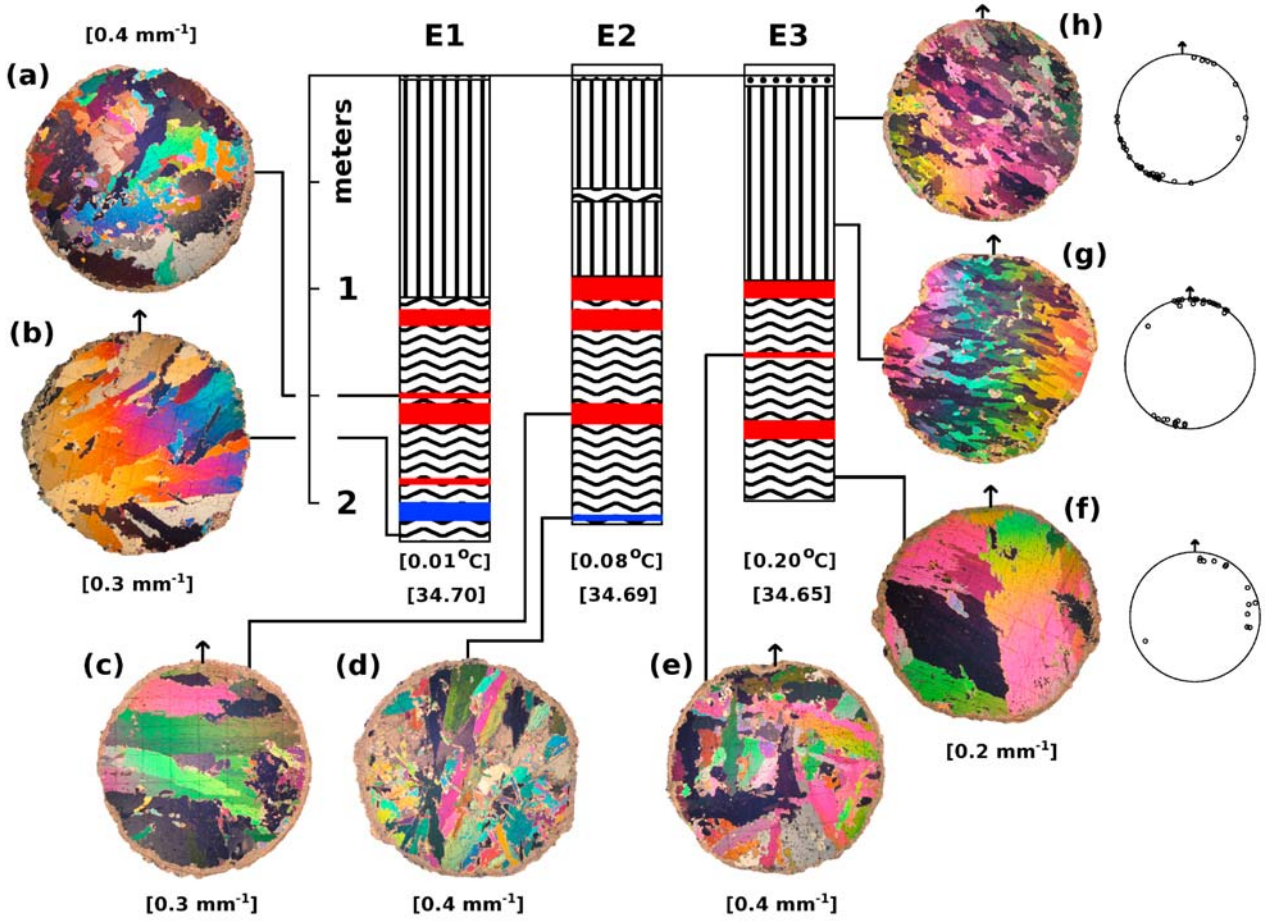

Figure 5. Ice composition summary and sample thin sections from eastern cores. (a) Draped platelet, (b) resumed columnar, (c) a mixture of draped platelet and resumed columnar, (d) bladed platelet, (e) draped platelet, (f) resumed columnar, and (g and h) moderately aligned columnar. Arrows mark north azimuth in selected thin sections and Schmidt nets. The deviation of the temperature from the in situ freezing point, averaged over the top 20 m of the water column, is presented below corresponding cores. Salinity averaged over the top 20 m of the water column is also shown. Where appropriate, B_A values for thin sections are included.

1998; *Jones and Hill*, 2001], is probably due to a combination of interannual variability, and differences in the classification of ice as columnar or platelet by different researchers. In addition, our east-west transect is not representative of the sea ice of the entire Sound.

[29] C axis measurements in the columnar ice at E3, presented in Figure 5, demonstrate the development of a uniaxial girdle distribution, indicating the influence of currents at the ice-water interface. Following *Weeks and Gow* [1978] the degree of alignment is quantified by the standard deviation, s_0, around the mean orientation, x_0. Over a depth of 0.5 m (from 0.2 to 0.7 m) s_0 decreases from 25° to 16°, both of which fall in the 'moderately aligned' category of *Weeks and Gow*'s [1978] scheme. However there is a clear indication of increasing alignment. Such preferred c axis orientation has been observed previously in McMurdo Sound by *Jeffries et al.* [1993], *Gow et al.* [1998], and *Jones and Hill* [2001]. The error in measuring the azimuth was 10°, which when combined with s_0 = 16°, gives a 95% confidence interval of [−25°, 47°] within which the true mean horizontal orientation is contained.

[30] The currents in McMurdo Sound are strongly tidal [*Robinson*, 2004; *Leonard et al.*, 2006]. Observations at 63 m depth at site E3 around the time the core was collected show the primary axis of the tidal flow is along the compass bearing of 49°. Considerable vertical shear in the currents was observed at a nearby location in McMurdo Sound in 2005 (C. L. Stevens et al., unpublished measurements, 2008). Hence here we expect the currents at the ice-water interface to be more northerly, i.e., rotated anticlockwise, than those observed at 63 m, making the orientation of the ocean currents similar to the crystal orientation in the ice core. This is consistent with other studies that indicate surface flow during periods of sea ice growth in eastern McMurdo Sound is dominantly in the north-south direction [*Gilmour et al.*, 1960; *Leonard et al.*, 2006].

3.3.3. Incorporated Platelet Ice: Draped and Bladed

[31] The definition of incorporated platelet ice used in this paper includes any horizontal section of ice that dis-

plays an areal percentage of platelet crystals greater than 10%. Due to the variety in grain size and shape within this classification we further define the subclasses of bladed platelet ice, draped platelet ice and resumed columnar ice. Presumably the characteristics of these fabrics reflect variations in the conditions in which the incorporated platelet ice forms; such as the degree of supercooling in the water column, or the magnitude of the flux of loose platelets relative to the rate of advance of the ice-water interface.

[32] The eastern cores display columnar to incorporated platelet transitions at approximately 1 m depth (see Figure 5). In the western cores the transition from granular ice in the upper layer to incorporated platelet ice occurs between 0.5 and 1.0 m depth in the core.

[33] In each case the transition from columnar or granular to incorporated platelet ice occurs relatively abruptly over a depth of 20–30 mm. Buoyancy arguments, suggested by the simulations of section 5.3, indicate that the first platelet crystals arriving at the approximately flat ice-water interface should orient with vertical c axes, i.e., with their basal plane parallel to the base of the sea ice cover. A directed, high-density, horizontal thin sectioning experiment over this fabric transition carried out in the same area in 2008 implied such crystals may be present (A. Gough, personal communication, 2008). However, such an experiment was not possible in the present study.

[34] Draped platelet fabric, previously reported in McMurdo Sound by *Jeffries et al.* [1993] and at Hells Gate Ice Shelf by *Tison et al.* [1998], is observed in vertical thin sections and characterized by centimeter-sized crystals. In some instances the crystals exhibit fluted grain boundaries, defined here as millimeter-scale variations in grain boundary position. *Tison et al.* [1998] suggest that this fabric may be due to a variable amount of supercooling in the ice shelf water from which the platelets are presumed to form. Draped platelet ice is observed in cores from W1, E1, E2 and E3 in the top and middle portions of the incorporated platelet layer (see Figures 4 and 5). Absence of this ice type from W2 and W3 may be due to the different growth conditions in the area. The origins of draped platelet ice and fluted grain boundaries are explored in a high-density thin sectioning experiment reported by *Dempsey* [2008].

[35] Bladed platelet fabric has previously been reported (though not termed as such) in McMurdo Sound [*Gow et al.*, 1998], Hells Gate Ice Shelf [*Tison et al.*, 1998], and the Weddell Sea [*Eicken and Lange*, 1989]. This ice type is observed in cores from W1, W2, W3, E1 and E2, occasionally in the middle, but generally at the bottom of the incorporated platelet ice layer (see Figures 4 and 5). There is no apparent distinction in c axis distribution between draped and bladed platelet ice: both have a Schmidt net with randomly distributed points (see Figure 4).

3.3.4. Incorporated Platelet Ice: Resumed Columnar Ice

[36] The resumed columnar texture is classified as platelet ice because it can only exist beneath platelet ice. The texture displays vertically and horizontally extensive crystals of lamellar texture (characteristic of constitutional supercooling) that appear beneath some form of incorporated platelet ice, i.e., draped or bladed platelet ice. Resumed columnar growth has been observed in the three eastern cores with individual crystals having horizontal dimensions of 20 mm parallel to the c axis and more than 80 mm perpendicular to the c axis (see Figure 5f). These dimensions are in contrast to the columnar ice where crystals have dimensions 3–6 mm parallel to the c axis and up to several 10's of mm perpendicular to it. The c axis orientations of the resumed columnar crystals are generally inclined between 0° to 30° from the horizontal. The lamellar texture of these crystals indicates that growth has occurred in situ, rather than from advection of ice crystals into the location.

[37] We hypothesize that resumed columnar crystals form due to geometric selection from a subice platelet layer after the arrival of new ice crystals to the layer from the water column has ceased. Freezing is driven by heat flux to the atmosphere. The horizontal cross-sectional area of crystals expands rapidly at first until c axes are predominantly horizontal and competition is lessened [*Gray*, 1984]. The larger cross section of resumed columnar crystals, relative to columnar ice formed before platelet ice appears, is attributed to the larger grain size of the initial layer from which it grew: granular ice develops into smaller grained, columnar sea ice; larger platelets of a subice platelet layer develop into larger grained, resumed columnar sea ice. This growth mechanism is further explored in section 5.2.

[38] The mechanism for resumed columnar growth requires that the flux of loose platelet crystals contributing to the subice platelet layer is reduced such that it does not interfere with geometric selection. We suggest that the appearance of resumed columnar texture in a core indicates the end of a supply of ice crystals from the ocean.

4. Numerical Simulation

4.1. Overview

[39] A 3-D model is constructed that focuses on modeling the development of crystal texture and fabric. The model simulates the accumulation of a subice platelet layer through the arrival of loose platelet crystals from the water column and the incorporation of this layer into a thickening, overlying ice sheet, producing incorporated platelet ice. It allows exploration of the cause and effect relationships inherent in these processes and deepens our understanding of how the final structure of incorporated platelet ice reflects aspects of its growth history.

[40] The model is primarily concerned with the mechanics of platelet ice processes. In particular, attention is paid to (1) the translations and rotations that take place as a buoyant loose platelet crystal arrives and settles into a platelet layer; (2) the in situ growth of distinct platelet crystals while they are members of the subice platelet layer; and (3) the incorporation of the subice platelet layer into the overlying sea ice cover by an advancing interface. Some aspects of fluid dynamics are treated indirectly by manipulating the initial conditions for the arrival of loose platelets.

[41] The model seeks to simulate 50 to 100 mm of ice growth at the base of a previously established sea ice cover. In these circumstances the growth rate will be approximately constant and the sample may be regarded as isothermal, with temperature variations of less than 1 K. Consequently the treatment of the thermodynamics of platelet and sea ice processes is excluded from the model for simplicity and to

allow simulations of greater resolution. The simulated interface advance is not driven by a temperature gradient but rather is set at a constant rate matching field observations made by *Purdie et al.* [2006]. Similarly the growth rate of individual platelets in the platelet layer is neither depth dependent nor driven by a variable supercooling but, again, set at a constant rate. The treatment of salinity is simple enough to ensure mass conservation and to prevent runaway crystal growth into large brine inclusions, but not complex enough to yield meaningful predictions for a salinity profile shape in the incorporated platelet ice. The model does not reproduce the morphological instability of an advancing columnar interface. This has been the focus of studies by *Kawano and Ohashi* [2008, 2009].

[42] The emphasis on mechanics at the expense of thermodynamics lends the model to certain types of predictions and not to others. In particular, the crystallographic properties of grain boundary density and c axis distribution are, respectively, a measure of the size and number density of incorporated platelets, and the spatial orientation of platelets, which are largely determined by the mechanical processes we have treated here. Conversely, salinity, temperature and brine volume profiles, which are mainly thermodynamic in nature, are not considered in this work.

4.2. Model Details

[43] The model uses an iterative technique called Voronoi dynamics [*Ohashi et al.*, 2004] to grow an ensemble of ice platelets in a 3-D environment. This method has been used by *Kawano and Ohashi* [2006] to simulate columnar ice growth in two and three dimensions, and has reproduced the cellular microstructure associated with this growth mode [*Kawano and Ohashi*, 2008, 2009]. The model described here was inspired by these elegant simulations but has been constructed independently of the Kawano and Ohashi model.

[44] The domain in which virtual ice is grown is a three dimensional array with cell indices, $\mathbf{x}$, as spatial coordinates. Cell elements, $D(\mathbf{x}, t)$, denote the presence of seawater, ice or brine at position $\mathbf{x}$ at time t. Arbitrarily, a 1 defines a cell, or pixel, as seawater (salinity 35), a -2 as brine (salinity 42 corresponding to an in situ temperature of -2.3°C), and an identification number between 0.05 and 0.95 is assigned to pixels belonging to each distinct platelet crystal. There is a trade-off between the number of independently growing platelet crystals, N, and the domain resolution, which is generally 200 cell widths or less in each dimension. In addition to the growth of individual platelets, a steadily advancing planar interface may be included to represent platelet incorporation by interstitial columnar growth.

[45] A complete description of the method is given by *Dempsey* [2008], with an outline given here. For the ith independently growing platelet, a growth array, $G_i(\mathbf{x})$, and a distance array, $R_i(\mathbf{x})$, are constructed with the same dimensions as the domain. Elements in $R_i(\mathbf{x})$ store the coordinate distance between $\mathbf{x}$ and the location of the ith platelet's center of mass, $\mathbf{c}_i$. Elements in $G_i(\mathbf{x})$ represent the platelet growth velocity from $\mathbf{c}_i$ in the $\mathbf{x} - \mathbf{c}_i$ direction. To model the anisotropy in ice crystal growth rate, virtual platelet growth varies with direction from $\mathbf{c}_i$. However, the $G_i(\mathbf{x})$ is independent of time and depth.

[46] The governing equation of Voronoi dynamics [*Ohashi et al.*, 2004]

$$R_i(\mathbf{x}) - G_i(\mathbf{x})t < 0 \tag{1}$$

describes an expanding surface representing unconstrained growth of the ith platelet (Figure 6a). If at time, t, a domain pixel at $\mathbf{k}$ is contained by the expanding surface then $\mathbf{k}$ satisfies equation (1), i.e., $R_i(\mathbf{k}) - G_i(\mathbf{k})t < 0$. The pixel is switched to, say for the ith platelet, 0.4 providing it satisfies the following conditions. First, that the pixel is currently seawater, i.e., $D(\mathbf{k}) = 1$. Second, the pixel is adjacent to another pixel, $\mathbf{k}_{adj}$, belonging to the ith platelet, i.e., $D(\mathbf{k}_{adj}, t) = 0.4$. Thus, a platelet may not grow to consume another platelet or pocket of brine, and is constrained to grow on its own boundary. 'Growth' of a platelet is achieved by iteratively increasing t to $t + \Delta t$, which allows more pixels to satisfy equation (1). Δt must be chosen such that an iterative increase of t expands the surface defined by equation (1) by no more than one pixel width in any direction. Each of the N platelets takes a turn to grow upon time step advancement.

[47] Elements of $G_i(\mathbf{x})$ describe the shape of the ith platelet. Platelets derive their disk-like shape from the kinetics of ice growth in the basal and c axis directions [*Hillig*, 1959], parameterized in the model by growth rates g_b and g_c, respectively. Observations of loose platelets recovered from oceanographic access holes in McMurdo Sound indicate some complex, possibly dendritic, edge structure in the basal plane while growth parallel to the c axis is limited to 'thickening' of the platelet. Therefore, growth in these two directions is treated separately and the shape is controlled by the relative size of three parameters; g_b controls growth (in the basal plane) of a polygon with up to 15 sides; g_d parameterizes the rough growth perturbations around the platelet edge (see Figure 7) using a sinusoid as a first approximation; g_c controls the amount of growth parallel to the c axis. Previous models of frazil crystal populations have set the basal to c axis growth ratio between 50 and 100 [*Jenkins and Bombosch*, 1995; *Smedsrud and Jenkins*, 2004], while *Kawano and Ohashi* [2009] choose a value of 10. However, guided by observations of platelet thicknesses, this ratio has been set at 30 in this paper, except for sensitivity tests (see section 5.2 and Figure 9). All platelets within a simulation have identical values of g_b, g_d and g_c.

[48] Conservation of mass is ensured for water because pixels of liquid are converted directly to solid, their expansion on freezing being ignored. Salt mass is also conserved, although modeling of the inclusion of brine is rudimentary. At each iteration, we identify pockets of seawater that have been isolated from the ocean by platelet crystals or, if present, an advancing interface. Interface or platelet growth continues into a pocket, rejecting all salt from the ice formed, until the salinity reaches 42, corresponding to an ice temperature of -2.3°C. The pocket is then labeled as brine (relevant pixels are switched to -2) and no further growth may intrude.

[49] The settling of loose platelets beneath the bottom of a subice platelet layer may influence the c axis distribution and grain boundary density of the resulting incorporated platelet ice. In this model a platelet arrival event involves

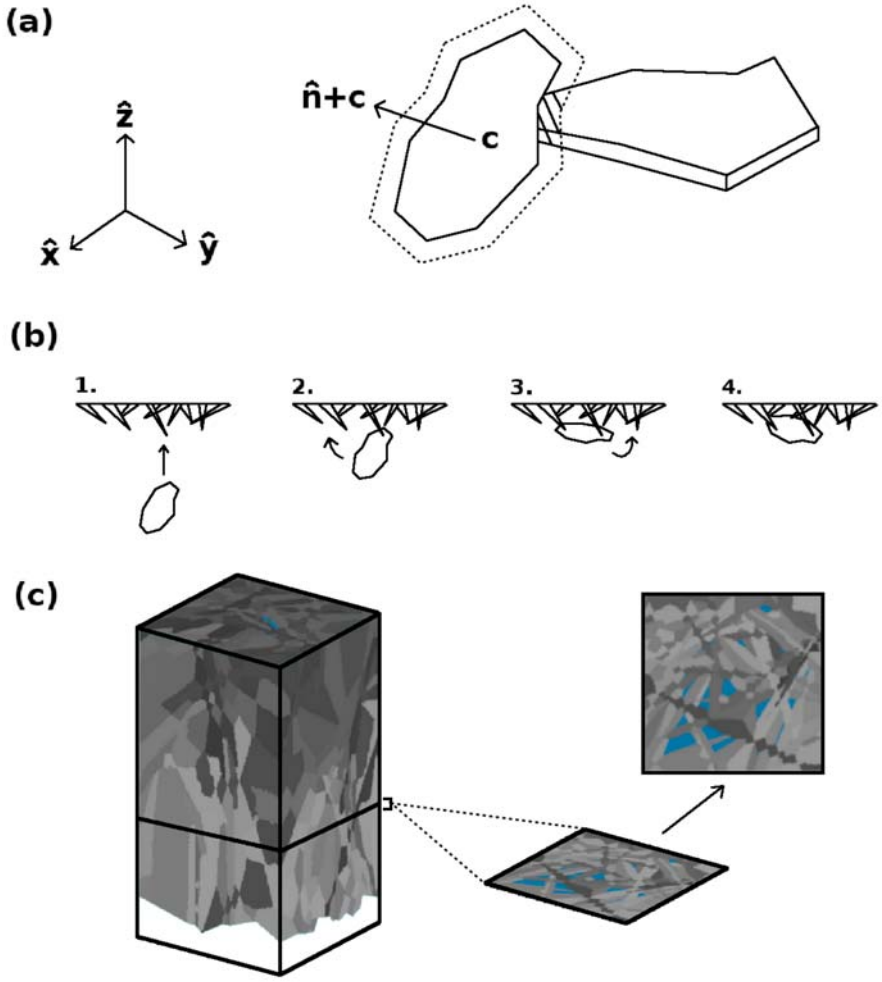

Figure 6. Pictorial representation of simulation dynamics. (a) Growth of a platelet centered at **c** with c axis $\hat{\mathbf{n}}$. At time t, the platelet occupies points satisfying $R(\mathbf{x}) - G(\mathbf{x})t < 0$, contained by the solid line. Advancement to time $t + \Delta t$ increases platelet boundary to the dashed line, containing points satisfying $R(\mathbf{x}) - G(\mathbf{x})(t + \Delta t) < 0$. Shaded area indicates the region where growth is prohibited due to previous occupation by another crystal. (b) A platelet arrival event beginning with initial contact (1), followed by two rotations (2 and 3) before achieving mechanical stability (4). (c) Thin section extraction from a virtual volume of ice.

forecasting where a platelet, P, of some shape, orientation and location beneath the virtual ice, will eventually settle and attain mechanical stability. First, P is projected upward to the point of first ice contact in $D(\mathbf{x})$. It then pivots about this contact point until it makes contact a second time with ice in $D(\mathbf{x})$. P continues to pivot about pairs of contact points until the center of mass, **c**, is contained within a polygon formed by three or more contact points, the model condition for mechanical stability (Figure 6b). Sliding of P across contacts points is not allowed. Once in its final position beneath the ice, a growth function is constructed for P and pixels are switched to add P to $D(\mathbf{x}, t)$. The total platelet count is increased to $N + 1$.

[50] This mechanism for addition to the platelet layer does not directly include the effects of fluid dynamics or buoyancy on platelets, nor does it include the mechanical interactions between two platelets rising simultaneously. The average basal dimension of a platelet is parameterized by l and is a normally distributed quantity as suggested by the results of *Smedsrud and Jenkins* [2004] for frazil crystals in an ice shelf plume.

5. Comparisons of Observation With Simulation

5.1. Interpretation

[51] A virtual volume of ice produced by the model is investigated using techniques similar to those applied to ice cores collected from McMurdo Sound. Horizontal (Figure 8) and vertical thin sections are extracted as 2D matrices from $D(\mathbf{x})$ and displayed by assigning each pixel a color depending on its value (Figures 8 and 6c). C axis distributions, presented on a Schmidt net, and grain boundary densities are calculated for virtual horizontal thin sections. The set of points defining a c axis distribution is reduced to the two dimensionless coordinates $\ln(S_1/S_2)$ and $\ln(S_2/S_3)$, where $[S_1,S_2,S_3]$ are eigenvalues calculated for the distribution [*Woodcock*, 1977]. A c axis distribution is thus reduced to a point on a logarithmic two-axis ratio plot (see

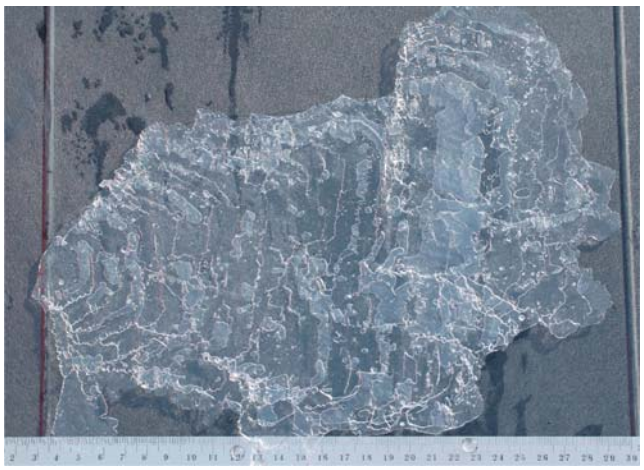

Figure 7. A large platelet recovered from a hole at W1. Knobbly, possibly dendritic, growth is evident around the edges. Scale is in cm.

Figure 10), where advance along the horizontal axis represents an increasingly pronounced girdle distribution, while larger values in the vertical correspond to more clustered distributions. Platelet fabrics with random distributions plot near the origin (see Figure 10, point d) while columnar fabrics, that are not aligned within the horizontal plane, plot close to the horizontal axis (Figure 10, point c). Columnar fabrics aligned by the influence of currents have both clustered and girdle components and thus plot nearer to the girdle/cluster transition (Figure 10, point a).

[52] Physical dimensions are applied by equating two model parameters, in computational units, to their natural counterparts, in physical units. For those simulations that model platelet arrival events, the average basal dimension, l, in pixels is equated to the average basal dimension of natural platelets upon their arrival at the interface and prior to in situ growth. Observations at the columnar-incorporated platelet ice transition indicate 4 mm is an appropriate estimate of this quantity (A. Gough, personal communication). Thus, spatial dimensions in the model (measured in pixels) are calibrated to physical units (in mm) by scaling by a factor of $\frac{4}{7}$. The computer time, t, is calibrated to physical time by equating model interface advance (in pixels per iteration) to the observed rate of interface advance in McMurdo Sound (approximately 10 mm d^{-1} during mid-winter [*Purdie et al.*, 2006]).

[53] In sections 5.2–5.7 we explore the influence of model parameters on the virtual platelet ice. In section 5.2 in situ crystal growth without a platelet flux from the water column is investigated. In section 5.3, we include this flux and examine platelet arrivals at a flat ice-water interface. In section 5.4 we model the effect of platelet orientation upon arrival at a subice platelet layer. In sections 5.5 and 5.6 in situ growth is switched off, while the characteristics of the platelet flux are explored: the influence of platelet size distribution is considered in section 5.5; and the magnitude of the platelet flux (relative to the rate of advance of the interface) is examined in section 5.6. Finally, in section 5.7, the influence of platelet flux and in situ growth on grain boundary density are explored. Where appropriate inferences are made using 2007 observations of McMurdo Sound sea ice.

5.2. Geometric Selection

[54] This well-documented behavior in growing sea ice provides a good test of the model and allows us to explore the effect of the anisotropy in platelet growth, as parame-

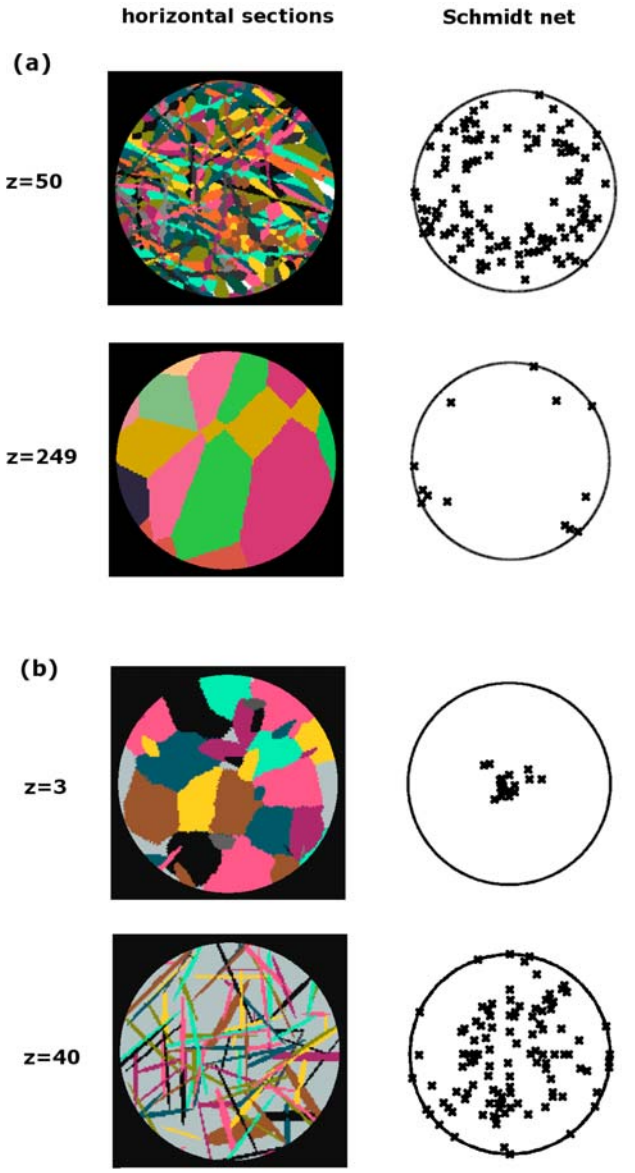

Figure 8. Horizontal thin sections and c axis distributions from simulated platelet ice. (a) Simulation of geometric selection, where colors indicate individual ice grains and white marks pockets of brine. Here $z = 50$ is near to the depth of crystal seeding and $z = 249$ demonstrates the evolution to resumed columnar ice by geometric selection. (b) Simulation of the rising and attachment of crystals to an initially planar ice-water interface, with colors indicating individual crystals and grey denoting interstitial columnar sea ice. Here $z = 3$ shows initial crystals at the planar ice-water interface, and $z = 40$ demonstrates the development of a disordered fabric deeper in the virtual ice.

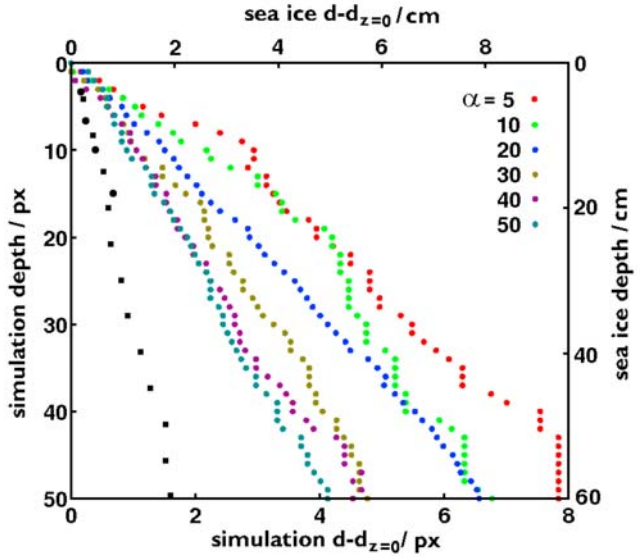

Figure 9. Grain size versus depth with growth anisotropy, $\alpha = g_b/g_c$, as the parameter. The data for $\alpha = 20$ are averaged over five simulations. These are compared with sea ice data collected from Thule, Greenland (solid squares), and Hokkaido, Japan (solid circles), from *Weeks and Ackley* [1982]. Aspect ratios are the same for both sets of axes.

terized by g_b/g_c. Traditional geometric selection in sea ice favors the development of columnar ice with horizontal c axes from randomly oriented granular ice. In the present simulations we model the growth of a collection of ice platelets nucleated at a given depth in the absence of loose platelet arrival from the water column (as in Figure 8a). We have hypothesized that this process produces resumed columnar fabric.

[55] The average grain dimension (relative to the initial average grain dimension), $d - d_{z=0}$, increases with depth (see Figure 9), for simulations in which the basal to c axis growth anisotropy is increased from 5 to 50. Computational units are not calibrated to their physical counterparts because simulations do not include platelet arrival events. We compare our data with columnar sea ice data from Greenland and Japan [*Weeks and Ackley*, 1982]. Geometric selection in natural sea ice yields an approximately linear increase in grain size with depth, which is successfully reproduced by our simulations. Also, it is evident that the slope is dependent on growth anisotropy. While g_b/g_c in the range 5 to 50 does not produce the gradient observed by *Weeks and Ackley* [1982], Figure 9 suggests that an increase to ~150, close to values used by *Jenkins and Bombosch* [1995], would bring our simulations into agreement with field measurements. However our main focus here is to simulate the incorporation of a loose layer of crystals into the sea ice cover. Therefore in this paper we choose $g_b/g_c = 30$ in agreement with our observations of loose platelets at the ice-water interface. This is thought to subsume processes such as flocculation [*Daly*, 2008] into this single parameter.

[56] The evolving c axis distribution subject to geometric selection for a simulation is presented as a path on a logarithmic two-axis ratio plot (solid line in Figure 10). Samples close to the depth of ice crystal 'nucleation' have random c axis distributions (for example as in Figure 8a) characteristic of granular or incorporated platelet ice and are plotted close to the origin. Two samples of incorporated platelet ice from the core at W1 also plotted near this location (Figure 10, point d). The path initially traverses approximately parallel to the horizontal axis indicating the development of a girdle fabric, which is consistent with geometric selection. Eventually the path moves toward a larger values of $\ln(S_1/S_2)$ indicating that some clustering is developing in addition to the girdle. This is a consequence of undersampling due to grain cross sections approaching total thin section area. The path terminates as it moves toward a c axis distribution (Figure 10, point c) observed at the bottom of the ice at E3 (see Figure 5f), which has been identified as resumed columnar ice.

5.3. Platelet Arrival and Its Influence on Interface Morphology

[57] The development of a subice platelet layer beneath the sea ice is probably concurrent with the arrival of scatterers in the water column, interpreted as a flux of buoyant platelet crystals [*Leonard et al.*, 2006]. If it is assumed these initial platelets are large compared to the length scale associated with the lamellar interface (~1 mm) then the interface may be regarded as 'flat' and the presence of buoyant forces would suggest they should settle with basal planes parallel to the interface, i.e., with vertical c axes. It is then not obvious that a disordered c axis distribution, as observed in the video imagery of *Smith* [2001], *Leonard et al.* [2006], and in our 2007 observations, should evolve in the subice platelet layer.

[58] To investigate how such a disordered fabric might evolve, the rising and attachment of crystals to an initially planar and stationary ice-water interface has been simulated. Following the development of a subice platelet layer the ice-water interface advanced to terminate platelet growth and restrict the simulation runtime. As expected, the first crystals to encounter the interface oriented themselves with vertical c axes (see Figure 8b at $z = 3$), thus producing a 'step' in the otherwise planar ice-water interface. Successive arriving platelets tilted against these steps resulting in a deviation of the c axis away from the vertical (see Figure 8b at $z = 40$), and contributing to further unevenness at the interface.

[59] The dashed path plotted in the logarithmic two-axis ratio plot (Figure 10) shows rapid development of a random c axis subice platelet layer by this mechanism. The path begins in the strongly clustered region (at $\ln(S_1/S_2) \approx 6$) as expected for the predominantly vertical c axes of the first platelets to arrive at the interface. Over a depth of 15 pixels (px; or 13 mm), the path moves below $\ln(S_1/S_3) = 3$ and the fabric is random. At a depth of 30 px (or 25 mm) the path has reached the girdle/cluster transition and there is no indication of a preferred c axis orientation.

5.4. Rising Platelet Orientation

[60] *Field et al.* [1997] studied the dynamics of falling disks in a quiescent fluid and determined four modes of tumbling depending on the dimensionless moment of inertia, $I^* = \pi\rho t/64\rho_f d$, and the Reynolds number, $Re = ud/\nu$, of the disks, where t is the disk thickness, d is the disk diameter, u is the rise velocity, ν is the kinematic viscosity,

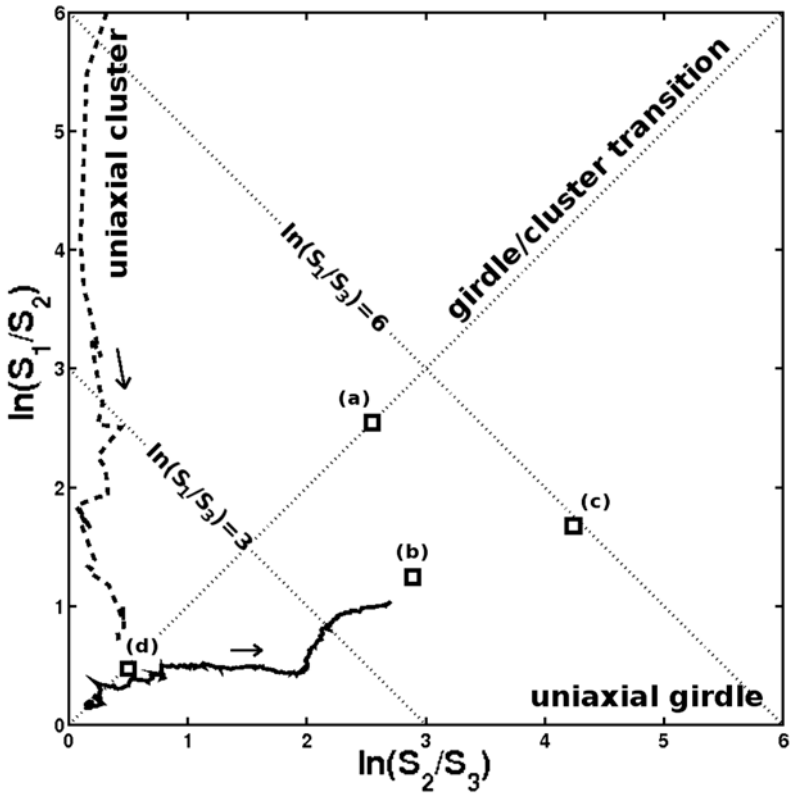

Figure 10. Solid line tracks the geometric selection simulation with the arrow pointing down the core. Dashed line simulates the formation of a platelet layer from a flat interface, arrow pointing down the core. Selected c axis distributions from McMurdo Sound ice marked moderately aligned columnar at 0.70 m depth at E3 (point a), moderately aligned columnar at 0.20 m depth at E3 (point b), resumed columnar from 1.88 m depth at E3 (point c), and incorporated platelet ice from 0.62 m and 1.96 m depth at W1 (point d).

and ρ and ρ_f are the density of the disk and fluid, respectively. Estimates of these parameters for the present work (d = 4 mm, t/d = 1/30, u = 1.5 cm s^{-1} [*Morse and Richard*, 2008], $\nu = 1.8 \times 10^{-6}$ m^{2}s^{-1}, and $\rho/\rho_f = 0.934$) suggest $I^* \approx 1.5 \times 10^{-3}$ and $Re \approx 30$, which implies platelets rise steadily, with a c axis inclination (from horizontal) between 80° and 90° [*Field et al.*, 1997]. Upon first contact with the subice platelet layer this mode predominantly presents platelets with near vertical c axes. However, other orientations at impact are possible because of turbulence in the water column.

[61] Figure 11 summarizes the results of simulations for platelets that have made initial contact with the subice platelet layer with c axes selected randomly from within bins [0°–10°], [0°–30°], [0°–90°], [60°–90°] and [80°–90°]. There is no apparent relationship between the c axis inclinations of the rising platelets and the measurable crystallographic properties of grain boundary density or average c axis inclination in the incorporated platelet ice. Conversely, this suggests that the behavior of platelets as they rise to the interface in still or moving water cannot be inferred from the crystallographic properties of incorporated platelet ice.

5.5. Crystal Packing Efficiency

[62] It is useful at this stage to consider the influence of platelet size distribution on the solid volume fraction in the subice platelet layer. In McMurdo Sound this has been estimated to be approximately 20% [*Bunt and Lee*, 1970]. Solid fraction is the result of (1) initial platelet arrival to the subice platelet layer, (2) in situ growth of platelets in the layer, and (3) secondary movement of platelets in the layer due to currents at the interface and increased buoyancy forces with accumulation. Process 3 has not been modeled in the present paper. Further, in simulations investigating solid fraction, in situ platelet growth (process 2) has also be omitted, in order to permit large numbers of platelets to be simulated, i.e., $N \sim 10^4$. Thus the packing efficiency, β, which is calculated only accounts for initial platelet arrival at the interface and is an underestimate of the solid fraction through most of the layer.

[63] The set of simulations which produce an estimate for β uses a 300 × 300 × 200 px^3 domain filled by loose platelets in the absence of an advancing interface, where platelet diameters range from 12–50 px. An interior volume of the resulting ice is selected to avoid boundary effects and β calculated as the proportion of the selected pixels denoting ice. The results, summarized in Table 3, suggest no apparent dependence of β on either the mean or the standard deviation of the size distribution of the arriving platelets. As expected, these β are considerably lower than the 20% observed in McMurdo Sound and the difference is attributed to in situ platelet growth and secondary platelet movement (processes 2 and 3).

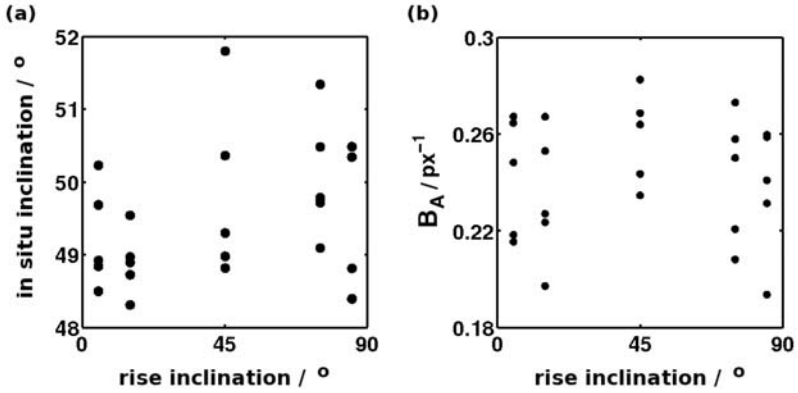

Figure 11. Subice platelet layer response to various platelet rise modes. (a) Mean in situ c axis inclination of platelets against average c axis inclination of rising platelets and (b) average B_A over the depth of platelet arrival to the subice platelet layer against average c axis inclination of rising platelets. Note that 0° indicates a horizontal c axis and 90° indicates a vertical c axis.

5.6. Platelet Flux and Subice Platelet Layer Development

[64] In this section a set of simulations investigates the platelet flux required to produce a loose, under ice platelet layer when in competition with an advancing ice-water interface. If the flux is below some critical value, platelets settle at the interface with vertical c axes (as in section 5.3) and are engulfed by the advancing interface before their unevenness contributes to the development of a subice platelet layer. Again, in situ growth of platelets is not simulated in favor of large platelet numbers, i.e., $N \sim 10^4$.

[65] We define z_{pl} as the approximate depth of the subice platelet layer and propose as a first approximation to its rate of advance

$$\frac{dz_{pl}}{dt} = \frac{1}{A}\frac{dN}{dt}\frac{V}{\beta} = \Phi\frac{V}{\beta}, \tag{2}$$

where $\Phi = \frac{1}{A}\frac{dN}{dt}$ is the platelet flux and V is the average volume of a single ellipsoidal platelet of average basal dimension l and aspect ratio $\alpha = \frac{g_b}{g_c}$. Hence, V/β is a modified platelet volume that accounts for the average volume of seawater surrounding each platelet in the layer. If the ice-water interface depth, z_{int}, advances at $\frac{dz_{int}}{dt}$, then a subice platelet layer will form when the condition

$$\frac{dz_{pl}}{dt} > \frac{dz_{int}}{dt} \tag{3}$$

is satisfied. This corresponds to the platelet flux being greater than some critical value, i.e.,

$$\Phi > \Phi_{crit}, \quad \text{where} \quad \Phi_{crit} = \frac{\beta}{V}\frac{dz_{int}}{dt}. \tag{4}$$

For $V = \frac{4}{3}\pi(l/2)^3/\alpha = 1.1 \times 10^{-9}$ m^3, an estimated β between 0.05 and 0.07 (see Table 3), and an interface advancement rate of 10 mm d^{-1} [*Purdie et al.*, 2006], equation (4) produces [4.5, 6.3] $\times 10^5$ platelets m^{-2} d^{-1} as a bounding interval for Φ_{crit}. Using this set of parameters, simulations show that a subice platelet layer forms when $\Phi > 5.4 \times 10^5$. In natural subice platelet layers, packing efficiency is replaced by solid fraction and this is probably closer to 0.2 [*Bunt and Lee*, 1970]. For platelets with a basal dimension of 4 mm, equation (4) then yields a critical platelet flux of 1.6×10^6 platelets m^{-2} d^{-1}. This is an estimate for the lower bound on the platelet flux at the time of platelet layer formation. For a subice platelet layer to form earlier in the growth season when $\frac{dz_{int}}{dt}$ is higher, this critical platelet flux must be greater. A consequence of this result is that subice platelet layers are more likely to form later in the growth season.

5.7. Grain Boundary Density

[66] The response of the grain boundary density, B_A, is explored for two distinct growth processes; geometric selection during growth from the base of the subice platelet layer in the absence of a loose platelet flux; and the incorporation of a subice platelet layer that is subject to a flux of loose platelet crystals.

[67] Figure 12 presents the profile of B_A during a geometric selection simulation. B_A decreases smoothly with depth, which is a direct result of increasing average grain size and decreasing crystal number density (compare with Figure 9).

[68] The response of B_A to a platelet flux is examined in the next series of simulations. A pregrown subice platelet layer is used allowing for a maximum of 150 platelet arrival events and subsequent in situ growth. Platelets are added at rates between 3 per iteration and 1 per 3 iterations and an advancing ice-water interface is included at a constant rate of 0.5 px per iteration. B_A is averaged over the depth of ice

Table 3. Packing Efficiencies for Accumulating Platelet Size Distributions[a]

Simulation	μ (px)	σ (px)	β (%)
1	12	2	6.4
2	20	2	5.3
3	20	2	5.6
4	30	10	6.8
5	40	15	7.8
6	50	15	4.8
7	10	5	6.1

[a]Here β is the packing efficiency, μ is the mean, and σ is the standard deviation of the accumulating platelet size distributions.

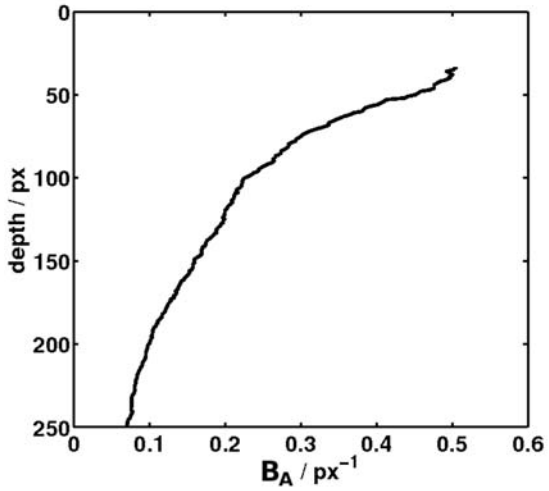

Figure 12. Grain boundary density, B_A, profile for a geometric selection simulation produced from 150 seed crystals. Platelets were seeded at a depth of ~30 px, which is the depth of maximum B_A and allowed to grow down until the simulation space was filled.

that receives platelets (treating interface-grown ice as a single grain) and plotted against the ratio of platelet flux to the rate of interface advance (see Figure 13). For platelet-interface ratios less than 6×10^{-5}, B_A responds positively to a relative increase in platelet flux. For values of this ratio greater than 6×10^{-5} the line of best fit though the points has gradient which includes zero ($(1.27 \pm 1.29) \times 10^3$ mm^{-1}); that is, there is no evidence to suggest that B_A depends on platelet flux for large fluxes.

[69] Provided the contribution of interstitial columnar ice can be regarded as constant, Figure 13 suggests that a study of B_A in incorporated platelet ice may be used as a proxy for platelet number density and thus is a qualitative indication of platelet flux [*Dempsey*, 2008]. Consideration of the effects of geometric selection and platelet flux, along with selected values of B_A from cores presented in Figures 4 and 5, provide insight into the nature of subice platelet conditions throughout the 2007 growth season. Cores from W1–W3 and E2 (see Figures 4 and 5) show an increasing B_A with depth indicating a relative increase in the loose platelet flux feeding the subice platelet layer. This increase is particularly obvious for thin sections of core W2 (Figure 4), where it is noted that a number of horizontally extensive platelet grains exist at 1.36 m depth and are entirely absent at 1.59 m depth. In contrast, sections from E1 and E3 (Figure 5) show decreasing grain boundary density with depth, which is attributed to the termination of the loose platelet flux and the resumption of geometric selection (as demonstrated in Figure 12). Note that this inferred distribution of platelet flux is reflected in the measured supercooling in the upper ocean, with the top 20 m of the water column being below the in situ freezing point at W1 and W2, and above it at other sites (see Figures 4 and 5).

6. Conclusion

[70] Crystallographic observations in McMurdo Sound are compared with numerical simulations of crystal texture and c axis distribution. The model replicates the mechanical processes that are believed to be important in the formation of platelet ice. These comparisons allow us to draw conclusions about the conditions which prevailed at the time of ice formation from the properties of the sampled incorporated platelet ice.

[71] First, the model is validated by reproducing geometric selection and demonstrating that a fit to sea ice observations would be possible by adjustment of the growth anisotropy within a physically reasonable range. The simulated increase in crystal size matches the behavior in natural ice and allows us to hypothesize that resumed columnar growth is a fabric that appears after the flux of loose platelets from the ocean has ceased. This ice type is mostly observed on the eastern side of the sound.

[72] This distribution of resumed columnar ice is consistent with the pattern of observed and simulated grain boundary densities, B_A. As indicated by the core analysis, B_A at the base of cores from the western part of our transect is higher than from cores taken along the eastern part. One outcome of the model is that a larger B_A is correlated with a larger platelet flux from the ocean. Indirect observations of a subice platelet layer beneath W1–W3, and the absence of such a layer beneath E1–E3 at the time of sampling, strengthen this conjecture. Thus we may conclude that the distribution in Figure 1, in addition to representing incorporated platelet ice, also parameterizes the thickness distribution of a subice platelet layer in McMurdo Sound. As might be expected, this deduced platelet layer thickness distribution is consistent with the pattern of in situ supercooling in the upper ocean measured in November 2007 (see Figures 4 and 5).

[73] The model identifies that the propensity for the formation of such a subice platelet layer depends on the relative magnitudes of the platelet flux and the rate of advance of the ice-water interface. This layer is more likely to form later in the growth season when the rate of advance of the ice-water interface has decreased, consistent with anecdotal reports of thicker layers in late spring. Further, the

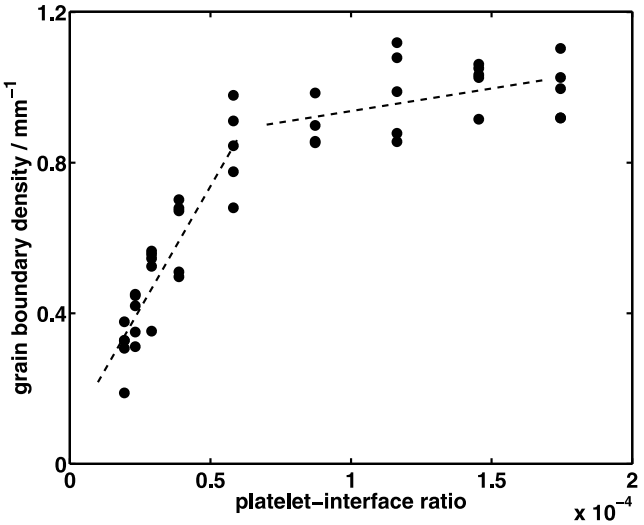

Figure 13. Grain boundary density, B_A, within arrival zone versus ratio of platelet flux to rate of advance of the ice-water interface.

simulation demonstrates how a disordered subice platelet layer results from an initially flat ice-water interface beneath the sea ice cover. It also establishes that there is no link between mode of rise of loose platelets in the water column and the c axis distribution of the resulting incorporated platelet ice.

[74] However the largely mechanical model described in this paper has its limitations. While an estimate of the initial solid fraction of the platelet layer was obtained, an estimate of the temporal evolution of solid fraction and the resulting salinity profile in sea ice would require consideration of thermodynamic processes in the simulations. Further it is unable to distinguish draped and bladed platelet fabrics with the implication that their occurrence may depend on thermodynamic conditions. Clearly the inclusion of thermodynamics into the numerical simulation would improve the accuracy and scope of its predictions.

[75] **Acknowledgments.** We are grateful to Craig Stevens, Craig Purdie, Alex Gough, Gerrard Liddell, and Yoshiki Kawano for insightful discussions and to two anonymous reviewers for their comments on an earlier draft of this manuscript. Logistics support in Antarctica was capably provided by Antarctica New Zealand, the staff at Scott Base, and Johno Leitch. This study was funded by the Foundation for Research, Science and Technology "Adaptation to Climate Variability and Change" programme, University of Otago Postgraduate Award, the New Zealand Post Antarctic Scholarship, National Institute of Water and Atmospheric Research Ltd., and Industrial Research Ltd.

References

Barry, J. P. (1988), Hydrographic patterns in McMurdo Sound, Antarctica and their relationship to local benthic communities, *Polar Biol.*, *8*, 377–391.

Bunt, J. S., and C. C. Lee (1970), Seasonal primary production in Antarctic sea ice at McMurdo Sound in 1967, *J. Mar. Res.*, *28*, 304–320.

Craven, M., F. Carsey, A. Behar, J. Matthews, R. Brand, A. Elcheikh, S. Hall, and A. Treverrow (2005), Borehole imagery of meteoric and marine ice layers in the Amery Ice Shelf, east Antarctica, *J. Glaciol.*, *51*(172), 75–83.

Craven, M., I. Allison, H. A. Fricker, and R. Warner (2009), Properties of a marine ice layer under the Amery Ice Shelf, east Antarctica, *J. Glaciol.*, *55*(192), 717–728.

Crocker, G. B., and P. Wadhams (1989), Modeling Antarctic fast-ice growth, *J. Glaciol.*, *35*(119), 3–8.

Daly, S. F. (2008), Evolution of frazil ice, *Proc. IAHR Int. Symp. Ice*, *19*, 29–47.

Dayton, P. K., G. A. Robilliard, and A. L. DeVries (1969), Anchor ice formation in McMurdo Sound, Antarctica, and its biological effects, *Science*, *163*, 273–274.

Dempsey, D. E. (2008), Observations and modeling of platelet ice in McMurdo Sound, Antarctica, M.Sc. thesis, Univ. of Otago, Dunedin, New Zealand.

Dieckmann, G., G. Rohardt, H. Hellmer, and H. Kipfstuhl (1986), The occurrence of ice platelets at 250 m depth near the Filchner Ice Shelf and its significance for sea ice biology, *Deep Sea Res.*, *33*, 141–148.

Drewry, D. J., S. R. Jordan, and E. Jankowski (1982), Measured properties of the Antarctic ice sheet: Surface configuration, ice thickness, volume and bedrock characteristics, *Ann. Glaciol.*, *3*, 83–91.

Eicken, H. (1992), Salinity profiles of Antarctic sea ice: Field data and model results, *J. Geophys. Res.*, *97*(C10), 15,545–15,557.

Eicken, H., and M. A. Lange (1989), Development and properties of sea ice in the coastal regime of the southeastern Weddell Sea, *J. Geophys. Res.*, *94*(C6), 8193–8206.

Eicken, H., H. Oerter, H. Miller, W. Graf, and J. Kipfstuhl (1994), Textural characteristics and impurity content of meteoric and marine ice in the Ronne Ice Shelf, Antarctica, *J. Glaciol.*, *40*(135), 386–398.

Field, S. B., M. Klaus, M. G. Moore, and F. Nori (1997), Chaotic dynamics of falling disks, *Nature*, *388*, 252–254.

Foldvik, A., and T. Kvinge (1974), Conditional instability of seawater at the freezing point, *Deep Sea Res.*, *21*, 169–174.

Gray, N. H. (1984), Geometric selection in two-dimensional crystal aggregates, *Math. Geol.*, *16*(1), 91–100.

Gilmour, A. E., R. J. P. Macdonald, and F. G. Van Der Hoeven (1960), Ocean currents in McMurdo Sound, *Nature*, *187*(4740), 867.

Gow, A. J., S. F. Ackley, J. W. Govoni, and W. F. Weeks (1998), Physical and structural properties of landfast sea ice in McMurdo Sound, Antarctica, in *Antarctic Sea Ice: Physical Processes, Interactions, and Variability*, *Antarct. Res. Ser.*, vol. 74, edited by M. O. Jeffries, pp. 355–374, AGU, Washington, D. C.

Hellmer, H. H. (2004), Impact of Antarctic ice shelf basal melting on sea ice and deep ocean properties, *Geophys. Res. Lett.*, *31*, L10307, doi:10.1029/2004GL019506.

Hillig, W. B. (1959), Kinetics of solidification from nonmetallic liquids, in *Kinetics of High-Temperature Processes*, edited by W. D. Kingery, pp. 127–135, MIT Press, Cambridge, Mass.

Hodgson, T. V. (1907), On collecting in Antarctic seas, in *British National Antarctic Expedition, 1901–1904*, vol. 3, *Zoology and Botany*, pp. 1–10, Trustees of the Brit. Mus., London.

Jeffries, M. O., W. F. Weeks, R. Shaw, and K. Morris (1993), Structural characteristics of congelation and platelet ice and their role in the development of Antarctic land-fast sea ice, *J. Glaciol.*, *39*(132), 223–238.

Jeffries, M. O., R. A. Shaw, K. Morris, A. L. Veazey, and H. R. Krouse (1994), Crystal structure, stable isotopes (δ^{18}O), and development of sea ice in the Ross, Amundsen, and Bellingshausen seas, Antarctica, *J. Geophys. Res.*, *99*(C1), 985–995.

Jeffries, M. O., A. P. Worby, K. Morris, and W. F. Weeks (1997), Seasonal variations in the properties and structural composition of sea ice and snow cover in the Bellingshausen and Amundsen seas, Antarctica, *J. Glaciol.*, *43*(143), 138–151.

Jeffries, M. O., H. R. Krouse, B. Hurst-Cushing, and T. Maksym (2001), Snow-ice accretion and snow cover depletion on Antarctic first-year sea-ice floes, *Ann. Glaciol.*, *33*, 51–60.

Jenkins, A., and A. Bombosch (1995), Modeling the effects of frazil ice crystals on the dynamics and thermodynamics of Ice Shelf Water plumes, *J. Geophys. Res.*, *100*, 6967–6981.

Jones, S. J., and B. Hill (2001), Structure of sea ice in McMurdo Sound, Antarctica, *Ann. Glaciol.*, *33*, 5–12.

Kawano, Y., and T. Ohashi (2006), Numerical simulation of development of sea ice microstructure by Voronoi Dynamics technique, *Proc. IAHR Int. Symp. Ice*, *18*, 97–103.

Kawano, Y., and T. Ohashi (2008), Numerical simulation of development of sea ice microstructures under temperature gradient, *Proc. IAHR Int. Symp. Ice*, *19*, 625–633.

Kawano, Y., and T. Ohashi (2009), A mesoscopic numerical study of sea ice crystal growth and texture development, *Cold Reg. Sci. Technol.*, *57*, 39–48.

Lange, M. A., S. F. Ackley, P. Wadhams, G. S. Dieckmann, and H. Eicken (1989), Development of sea ice in the Weddell Sea, *Ann. Glaciol.*, *12*, 92–96.

Langhorne, P. J., and W. H. Robinson (1986), Alignment of crystals in sea ice due to fluid motion, *Cold Reg. Sci. Technol.*, *12*(2), 197–215.

Langhorne, P. J., C. R. Purdie, I. J. Smith, G. H. Leonard, E. W. Kempema, C. Petrich, M. A. Gribble, P. E. Bond, and T. G. Haskell (2006), Antarctic landfast sea ice: The role of platelet ice, *Proc. IAHR Int. Symp. Ice*, *18*, 285–292.

Langway, C. C., Jr. (1958), Ice fabrics and the universal stage, *Tech. Rep. 62*, Snow, Ice and Permafrost Res. Estab., Hanover, N. H.

Leonard, G. H., C. R. Purdie, P. J. Langhorne, T. G. Haskell, M. J. M. Williams, and R. D. Frew (2006), Observations of platelet ice growth and oceanographic conditions during the winter of 2003 in McMurdo Sound, Antarctica, *J. Geophys. Res.*, *111*, C04012, doi:10.1029/2005JC002952.

Lewis, E. L., and R. G. Perkin (1985), The winter oceanography of McMurdo Sound, Antarctica, in *Oceanology of the Antarctic Continental Shelf*, *Antarct. Res. Ser.*, vol. 43, edited by S. Jacobs, pp. 145–165, AGU, Washington, D. C.

Lewis, E. L., and R. G. Perkin (1986), Ice pumps and their rates, *J. Geophys. Res.*, *91*(C10), 11,756–11,762.

Littlepage, J. L. (1965), Oceanographic investigations of McMurdo Sound, Antarctica, 1965, in *Biology of the Antarctic Seas II*, *Antarct. Res. Ser.*, vol. 5, edited by G. Llano, pp. 1–37, AGU, Washington, D. C.

Martin, S. (1981), Frazil ice in rivers and oceans, *Ann. Rev. Fluid Mech.*, *13*, 379–397.

Maykut, G. A. (1986), The surface heat and mass balance, in *The Geophysics of Sea Ice*, *NATO Adv. Sci. Inst. Ser.*, vol. 146, edited by N. Untersteiner, pp. 395–463, Plenum, New York.

Morse, B., and M. Richard (2008), A field study of suspended frazil ice particles, *Cold Reg. Sci. Technol.*, *55*, 86–102, doi:10.1016/j.coldregions.2008.03.004.

Nakawo, M., and N. K. Sinha (1981), Growth rate and salinity profile of first year sea ice in the high Arctic, *J. Glaciol.*, *27*, 315–330.

Ohashi, T., M. Sasaki, and K. Yoshimura (2004), A numerical simulation of the development of ice-microstructures, *Proc. Int. Symp. Okhotsk Sea Ice*, *19*, 180–185.

Paige, R. A. (1966), Crystallographic studies of sea ice in McMurdo Sound, Antarctica, *Tech. Rep. R494*, 31 pp., U.S. Nav. Civ. Eng. Lab., Port Hueneme, Calif.

Penrose, J. D., M. Conde, and T. J. Pauly (1994), Acoustic detection of ice crystals in Antarctic waters, *J. Geophys. Res.*, *99*(C6), 12,573–12,580.

Purdie, C. R., P. J. Langhorne, G. H. Leonard, and T. G. Haskell (2006), Growth of first-year landfast Antarctic sea ice determined from winter temperature measurements, *Ann. Glaciol.*, *44*, 170–176.

Robinson, N. J. (2004), An oceanographic study of the cavity beneath the McMurdo Ice Shelf, Antarctica, M.Sc. thesis, Victoria Univ. of Wellington, Wellington.

Smedsrud, L. H., and A. Jenkins (2004), Frazil ice formation in an ice shelf water plume, *J. Geophys. Res.*, *109*, C03025, doi:10.1029/2003JC001851.

Smith, I. J. (2001), Platelet ice in McMurdo Sound, Antarctica, Ph.D. thesis, Univ. of Otago, Dunedin, New Zealand.

Smith, I. J., P. J. Langhorne, T. G. Haskell, H. J. Trodahl, R. Frew, and M. R. Vennell (2001), Platelet ice and the land-fast sea ice of McMurdo Sound, Antarctica, *Ann. Glaciol.*, *33*, 21–27.

Tison, J. L., R. D. Lorrain, A. Bouzette, M. Dini, A. Bondesan, and M. Stivenard (1998), Linking landfast sea ice variability to marine ice accretion at Hells Gate Ice Shelf, Ross Sea, in *Antarctic Sea Ice: Physical Processes, Interactions, and Variability*, *Antarct. Res. Ser.*, vol. 74, edited by M. O. Jeffries, pp. 375–407, AGU, Washington, D. C.

United Nations Educational, Scientific and Cultural Organization (1981), Tenth report of the joint panel on oceanographic tables and standards, *Tech. Pap. Mar. Sci. 36*, 29 pp., Paris.

Weeks, W. F., and S. F. Ackley (1982), *The Growth, Structure and Properties of Sea Ice*, *Cold Reg. Res. Eng. Lab. Monogr. Ser.*, vol. 82, Cold Reg. Res. and Eng. Lab., Hanover, N. H.

Weeks, W. F., and A. J. Gow (1978), Preferred crystal orientations in the fast ice along the margins of the Arctic Ocean, *J. Geophys. Res.*, *83*(C10), 5105–5121.

Woodcock, N. H. (1977), Specification of fabric shapes using an eigenvalue method, *Geol. Soc. Am. Bull.*, *88*, 1231–1236.

Worby, A. P., R. A. Massom, I. Allison, V. I. Lytle, and P. Heil (1998), East Antarctic sea ice: A review of its structure, properties and drift, in *Antarctic Sea Ice: Physical Processes, Interactions, and Variability*, *Antarct. Res. Ser.*, vol. 74, edited by M. O. Jeffries, pp. 41–67, AGU, Washington, D. C.

Wright, C. S., and R. E. Priestley (1922), *Glaciology: British (Terra Nova) Antarctic Expedition, 1910–1913*, Harrison, London.

D. E. Dempsey and P. J. Langhorne, Department of Physics, University of Otago, PO Box 56, Dunedin 9054, New Zealand. (pjl@physics.otago.ac.nz)

R. D. Frew, Department of Chemistry, University of Otago, PO Box 56, Dunedin 9054, New Zealand.

T. G. Haskell, Industrial Research Ltd., 69 Gracefield Rd., PO Box 31-310, Lower Hutt 5040, New Zealand.

N. J. Robinson and M. J. M. Williams, National Institute of Water and Atmospheric Research Ltd., Private Bag 14901, Wellington 6022, New Zealand.